Structural Control in Porous Cross-Linked Poly(methacrylate) Monoliths Using Supercritical Carbon Dioxide as a "Pressure-Adjustable" Porogenic Solvent

Andrew K. Hebb, Kazunobu Senoo, Rahila Bhat, and Andrew I. Cooper*

Donnan and Robert Robinson Laboratories, Department of Chemistry, University of Liverpool, Crown Street, Liverpool L69 3BX, United Kingdom

Received November 14, 2002. Revised Manuscript Received March 14, 2003

The synthesis of permanently porous, highly cross-linked, poly(methacrylate) resins using supercritical CO_2 is described. The pressure-adjustable solvent properties associated with supercritical fluid solvents are exploited to fine-tune the average pore size and surface area of the materials. It was found that the materials' properties varied in a discontinuous manner with respect to the CO_2 pressure. A minimum in the BET surface area (and a maximum in the pore diameter) was observed at a reaction pressure of approximately 2600 psi. These trends were rationalized by the fact that the mechanisms of nucleation, aggregation, and pore formation are highly sensitive to the nature of the porogenic solvent environment.

Introduction

Highly cross-linked, permanently porous polymers are useful in a wide range of applications.[1−9] Unlike lightly cross-linked "gel-type" polymers which become porous when swollen by solvents, more highly cross-linked polymers have a permanent porous structure which is formed during their preparation and persists in the dry state.[10] The internal porous morphology is characterized by interconnected channels (pores) which permeate the rigid, extensively cross-linked polymer matrix. These materials are often synthesized in the form of uniform beads by suspension polymerization.[11−18] This can lead to performance limitations in certain applications, notably the chromatographic separation of large molecules. The passage of molecules within the pores is typically controlled by diffusion. Diffusion constants for large molecules, such as proteins or synthetic polymers, are several orders of magnitude lower than those for small molecules, causing problems in applications such as chromatography where the separation efficiency is strongly dependent on mass transfer rates. Modern HPLC methods frequently involve columns packed with porous polymer beads.[19−21] The flow of the mobile phase between the beads through the large interstitial voids in the column is relatively unimpeded, whereas liquid present in the network of resin pores does not flow and remains stagnant. For large molecules, diffusional mass transfer rates between the interstitial voids and the pores may be very slow, thus causing peak broadening and necessitating low flow rates or longer columns. A promising approach to this problem has been the synthesis of continuous, porous "monolithic" polymers,[22,23] which have been developed for a variety of applications including HPLC,[24] high-performance membrane chromatography (HPMC),[25] capillary electrochromatography,[26−29] microfluidics,[4,9] molecular imprinting,[3] and

* To whom correspondence should be addressed. Phone: 44-1-51-794-3548. Fax: 44-1-51-794-3588. E-mail: aicooper@liv.ac.uk.

(1) Hodge, P.; Sherrington, D. C. *Syntheses and Separations using Functional Polymers*; Wiley: New York, 1989.
(2) Tripp, J. A.; Svec, F.; Fréchet, J. M. J. *J. Comb. Chem.* **2001**, *3*, 216−223.
(3) Whitcombe, M. J.; Vulfson, E. N. *Adv. Mater.* **2001**, *13*, 467−478.
(4) Yu, C.; Xu, M. C.; Svec, F.; Fréchet, J. M. J. *J Polym. Sci. Polym. Chem.* **2002**, *40*, 755−769.
(5) Zhou, X.; Xue, B.; Sun, Y. *Biotechnol. Prog.* **2001**, *17*, 1093−1098.
(6) Zhou, X.; Xue, B.; Bai, S.; Sun, Y. *Biochem. Eng. J.* **2002**, *11*, 13−17.
(7) Tripp, J. A.; Svec, F.; Fréchet, J. M. J. *J. Comb. Chem.* **2001**, *3*, 604−611.
(8) Burguete, M. I.; Fréchet, J. M. J.; Garcia-Verdugo, E.; Janco, M.; Luis, S. V.; Svec, F.; Vicent, M. J.; Xu, M. C. *Polym. Bull.* **2002**, *48*, 9−15.
(9) Rohr, T.; Yu, C.; Davey, M. H.; Svec, F.; Fréchet, J. M. J. *Electrophoresis* **2001**, *22*, 3959−3967.
(10) Sherrington, D. C. *Chem. Commun.* **1998**, 2275−2286.
(11) Yuan, H. G.; Kalfas, G.; Ray, W. H. *J. Macromol. Sci., Rev. Macromol. Chem. Phys.* **1991**, *C31*, 215−299.
(12) Arshady, R. *Colloid Polym. Sci.* **1992**, *270*, 717−732.
(13) Mayes, A. G.; Mosbach, K. *Anal. Chem.* **1996**, *68*, 3769−3774.
(14) Vivaldo-Lima, E.; Wood, P. E.; Hamielec, A. E.; Penlidis, A. *Ind. Eng. Chem. Res.* **1997**, *36*, 939−969.
(15) Lewandowski, K.; Svec, F.; Fréchet, J. M. J. *Chem. Mater.* **1998**, *10*, 385−391.
(16) Dowding, P. J.; Vincent, B. *Colloids Surf., A* **2000**, *161*, 259−269.
(17) Alesso, S. M.; Yu, Z. R.; Pears, D.; Worthington, P. A.; Luke, R. W. A.; Bradley, M. *J. Comb. Chem.* **2001**, *3*, 631−633.
(18) Rohr, T.; Knaus, S.; Gruber, H.; Sherrington, D. C. *Macromolecules* **2002**, *35*, 97−105.
(19) Lewandowski, K.; Murer, P.; Svec, F.; Fréchet, J. M. J. *Chem Commun* **1998**, 2237−2238.
(20) Murer, P.; Lewandowski, K.; Svec, F.; Fréchet, J. M. J. *Anal. Chem.* **1999**, *71*, 1278−1284.
(21) Xu, M. C.; Brahmachary, E.; Janco, M.; Ling, F. H.; Svec, F.; Fréchet, J. M. J. *J. Chromatogr. A* **2001**, *928*, 25−40.
(22) Svec, F.; Fréchet, J. M. J. *Science* **1996**, *273*, 205−211.
(23) Peters, E. C.; Svec, F.; Fréchet, J. M. J. *Adv. Mater.* **1999**, *11*, 1169−1181.
(24) Xie, S.; Svec, F.; Fréchet, J. M. J. *J. Chromatogr. A* **1997**, *775*, 65−72.
(25) Tennikov, M. B.; Gazdina, N. V.; Tennikova, T. B.; Svec, F. *J. Chromatogr. A* **1998**, *798*, 55−64.
(26) Peters, E. C.; Petro, M.; Svec, F.; Fréchet, J. M. J. *Anal. Chem.* **1997**, *69*, 3646−3649.

10.1021/cm020979i CCC: $25.00
Published on Web 00/00/0000 PAGE EST: 8.7

high-throughput bioreactors.[30] Typically, a mold is filled with a polymerization mixture containing a cross-linking monomer, functional comonomer(s), initiator, and a porogenic diluent. This mixture is then polymerized, either thermally or photochemically, to form a continuous porous monolith which conforms to the shape of the mold. Many systems have involved the free radical polymerization of methacrylate- or styrene-based cross-linkers, e.g., ethylene dimethacrylate (EDMA) or divinyl benzene (DVB). The porogenic diluent may be either solvating or nonsolvating in nature, and carefully chosen ternary solvent mixtures can be used to allow fine control of the porous properties of the monolithic polymers.[26−28,31] In some cases, materials have been optimized to incorporate a distribution of small, diffusive pores (<100 nm), interconnected with larger, flow-through pores with diameters in the range 700−2000 nm.[32] The large pores provide permeability through the monolith and also facilitate convection, thus greatly enhancing mass transport. A key advantage of this methodology is that the porous polymers can be prepared directly within a variety of different containment vessels, including wide-bore chromatography columns, narrow-bore capillaries, and microfluidic devices. There are also disadvantages associated with the monolith approach: for example, the synthesis is solvent intensive and it may be difficult to remove solvent residues from the continuous materials after polymerization. Furthermore, highly cross-linked, permanently porous polyacrylates are quite often brittle and easily damaged, thus necessitating suitable permanent containment to allow handling (e.g., in capillaries or columns).

Previously, we have described the synthesis of highly cross-linked porous polymer monoliths[33,34] and beads[35] using supercritical carbon dioxide ($scCO_2$) as the porogenic diluent. Carbon dioxide is an attractive solvent for polymer chemistry because it is inexpensive, nontoxic, and nonflammable.[36−38] Unlike conventional liquid solvents, supercritical fluids (SCFs) are highly compressible and the density (and therefore solvent properties) can be tuned over a wide range by varying pressure.[39] Moreover, SCFs revert to the gaseous state upon depressurization, simplifying the separation of solvent from solute and eliminating solvent residues. A disadvantage associated with the use of $scCO_2$ is that relatively high reaction pressures (800−5000 psi) may be required.[40] In addition to the synthesis of porous cross-linked vinyl polymers, $scCO_2$ has been used for the formation of aerogels,[41] microcellular polymer foams,[42−44] porous biopolymer composites,[45] and emulsion-templated "polyHIPE" materials.[46]

Our preliminary work showed that porous polymers could be formed in $scCO_2$ by the polymerization of cross-linking monomers such as EDMA and trimethylolpropane trimethacrylate (TRIM). At relatively low monomer concentrations (<30% w/v), nonporous microgel powders were observed.[47,48] At higher monomer concentrations (40−60% v/v), continuous porous polymer monoliths were produced.[33,34] These materials conformed to the shape of the reaction vessel (i.e., they were "molded"). For polymers formed from TRIM, an increase in monomer concentration led to a marked decrease in the median pore size and a corresponding increase in the specific surface area.[33] It was found that relatively small changes in the monomer concentration could lead to dramatic changes in the resulting polymer structure. Early results indicated that the CO_2 pressure also influenced the polymer morphology and we suggested that it might be possible to vary the pore size distribution by changing the pressure, which in turn changes the solvent strength of the supercritical medium.[33,34] In support of this, we demonstrated that the surface area of porous cross-linked polymer beads produced by suspension polymerization could be varied by changing the density of the supercritical porogen.[35] In this paper, we explore this idea in much greater detail and show that it is indeed possible to "fine-tune" the porous morphology in cross-linked polymer monoliths by changing the CO_2 density. Moreover, we show that the variation of polymer properties such as pore size, pore volume, and surface area show marked discontinuities as a function of CO_2 pressure which cannot readily be accounted for by simple models relating to the effect of solvent quality on phase separation.

In the literature on porous resins, the term "macroporous" is often used to refer to materials with permanent porosity in the dry state, irrespective of pore size. To avoid confusion, we have restricted our use of the terms micropore, mesopore, and macropore to the definitions recommended by IUPAC,[49] i.e., micropores <2 nm, mesopores 2−50 nm, and macropores >50 nm. When referring to porous structures in general, we have adopted the expression "permanently porous", as proposed by Rohr et al.[18]

(27) Peters, E. C.; Petro, M.; Svec, F.; Fréchet, J. M. J. *Anal. Chem.* **1998**, *70*, 2296−2302.
(28) Peters, E. C.; Petro, M.; Svec, F.; Fréchet, J. M. J. *Anal. Chem.* **1998**, *70*, 2288−2295.
(29) Schweitz, L.; Andersson, L. I.; Nilsson, S. *Anal. Chem.* **1997**, *69*, 1179−1183.
(30) Petro, M.; Svec, F.; Fréchet, J. M. J. *Biotechnol. Bioeng.* **1996**, *49*, 355−363.
(31) Santora, B. P.; Gagne, M. R.; Moloy, K. G.; Radu, N. S. *Macromolecules* **2001**, *34*, 658−661.
(32) Svec, F.; Fréchet, J. M. J. *Chem. Mater.* **1995**, *7*, 707−715.
(33) Cooper, A. I.; Wood, C. D.; Holmes, A. B. *Ind. Eng. Chem. Res.* **2000**, *39*, 4741−4744.
(34) Cooper, A. I.; Holmes, A. B. *Adv. Mater.* **1999**, *11*, 1270−1274.
(35) Wood, C. D.; Cooper, A. I. *Macromolecules* **2001**, *34*, 5−8.
(36) Kendall, J. L.; Canelas, D. A.; Young, J. L.; DeSimone, J. M. *Chem. Rev.* **1999**, *99*, 543−563.
(37) Cooper, A. I. *J. Mater. Chem.* **2000**, *10*, 207−234.
(38) Cooper, A. I. *Adv. Mater.* **2001**, *13*, 1111−1114.
(39) Jessop, P. G.; Leitner, W. *Chemical Synthesis Using Supercritical Fluids*; Wiley VCH: Weinheim, 1999.
(40) Wood, C. D.; Senoo, K.; Martin, C.; Cuellar, J.; Cooper, A. I. *Macromolecules* **2002**, *35*, 6743−6746.
(41) Loy, D. A.; Russick, E. M.; Yamanaka, S. A.; Baugher, B. M.; Shea, K. J. *Chem. Mater.* **1997**, *9*, 2264−2268.
(42) Parks, K. L.; Beckman, E. J. *Polym. Eng. Sci.* **1996**, *36*, 2404−2416.
(43) Parks, K. L.; Beckman, E. J. *Polym. Eng. Sci.* **1996**, *36*, 2417−2431.
(44) Shi, C.; Huang, Z.; Kilic, S.; Xu, J.; Enick, R. M.; Beckman, E. J.; Carr, A. J.; Melendez, R. E.; Hamilton, A. D. *Science* **1999**, *286*, 1540−1543.
(45) Howdle, S. M.; Watson, M. S.; Whitaker, M. J.; Popov, V. K.; Davies, M. C.; Mandel, F. S.; Wang, J. D.; Shakesheff, K. M. *Chem. Commun.* **2001**, 109−110.
(46) Butler, R.; Davies, C. M.; Cooper, A. I. *Adv. Mater.* **2001**, *13*, 1459−1463.
(47) Cooper, A. I.; Hems, W. P.; Holmes, A. B. *Macromol. Rapid Commun.* **1998**, *19*, 353−357.
(48) Cooper, A. I.; Hems, W. P.; Holmes, A. B. *Macromolecules* **1999**, *32*, 2156−2166.
(49) Sing, K. S. W.; Everett, D. H.; Haul, R. A. W.; Moscou, L.; Pierotti, R. A.; Rouquerol, J.; Siemieniewska, T. *Pure Appl. Chem.* **1985**, *57*, 603−619.

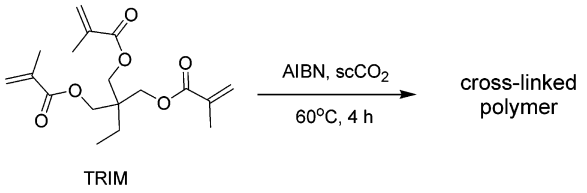

Figure 1. Synthesis of porous polyTRIM monoliths using $scCO_2$ as the porogenic solvent.

Experimental Section

Materials. Trimethylolpropane trimethacrylate (TRIM, Aldrich) was used as received. 2,2′-Azobisisobutyronitrile (AIBN) was recrystallized twice from methanol and dried under vacuum before use. Carbon dioxide (Messer Griesheim, Grade 5*5) was used as received.

Equipment. Liquid CO_2 was delivered to the reactor with a Pickel PM 101 nitrogen driven pump. The pressure in the reactor was measured with a pressure transducer (A105, RDP Electronics) and a digital display (E308, RDP Electronics). The internal reactor temperature was measured with an industrial mineral isolated thermocouple (Type K, RS Electronics). A PTFE-coated magnetic stir bar was used to mix the contents of the reactor before polymerization. The reactor was placed on its side such that the long axis was horizontal.

Polymerization. Reactions were carried out in a 10 cm^3 stainless steel view cell, as described previously.[48] Briefly, the monomer and the initiator were added to the reactor which was then purged with a slow stream of CO_2 for 10 min to remove any oxygen. CO_2 was then added to the reaction vessel and the mixture was stirred at room temperature until a single homogeneous phase was observed. The reactor was then heated to 60 °C (±0.5 °C) to initiate the polymerization. Phase behavior was observed through the sapphire window in the reaction vessel. The CO_2 was removed at the end of the reaction by depressurization. The rate of pressure release had no obvious influence on the polymer morphology as the materials were highly cross-linked and not subject to expansion or foaming.[42−45] No cracks were observed to form in the monolithic materials, even when the pressure was released quite rapidly. Monomer conversions were 95−100% in all cases.

Characterization. For analysis, the continuous polymer samples were fractured into millimeter-sized pieces with a scalpel. Pore size distributions were recorded by mercury intrusion porosimetry using a Micromeritics Autopore IV 9500 porosimeter. Samples were subjected to a pressure cycle starting at approximately 0.5 psia, increasing to 60 000 psia in predefined steps to give pore size/pore volume information. Polymer surface areas were measured using the BET method with a Micromeritics ASAP 2010 nitrogen adsorption analyzer. Samples were outgassed for 3 h at 60 °C under a N_2 flow before analysis. BET surface areas, pore volumes, and micropore surface areas (BJH) were calculated using the Micromeritics software package (version 5.0). Absolute densities were measured using a Micromeritics Helium AccuPyc 1330 pycnometer. Polymer morphologies were investigated with a Hitachi S-2460N scanning electron microscope (SEM). Samples were mounted on aluminum studs using adhesive graphite tape and sputter-coated with approximately 10 nm of gold before analysis. Atomic force microscopy was carried out using a Thermomicroscope Explorer AFM (SPMLAB Version 5.01 software). The set point voltage was adjusted between 45 and 50%. A standard silicon nitride probe with a 2646 N/m spring constant was used in tapping mode.

Results and Discussion

Pressure Changes During Polymerization. A series of experiments was conducted in which we synthesized porous polyTRIM monoliths (Figure 1) over a broad range of CO_2 pressures, as summarized in Table 1. Apart from the CO_2 pressure, all other variables (i.e., monomer volume, reactor volume, initiator concentration, heating rate, and reaction temperature) were kept constant. The lower pressure limit in these experiments was determined by the miscibility pressure for CO_2 and TRIM (i.e., the conditions at which TRIM and CO_2 formed a single homogeneous phase; this corresponds to a reaction pressure of about 1800−1900 psi at 60 °C). The maximum reaction pressure was limited by the safe working pressure for the apparatus. Figure 2a shows a representative plot of pressure versus time for one of these reactions (as recorded for sample 15, Table 1). Initially, there was a roughly linear increase in temperature with time over the course of about 1 h as the reactor was heated (Figure 2b). The pressure in the reactor increased in a similar fashion during heating and the ratio of pressure to temperature, P/T, was approximately constant during this period (Figure 2c). After about 65−70 min, a pale yellow color, quickly followed by a dark red color, was observed in the reactor due to light scattering that arises from the formation of primary microgel particles.[48] Between 70 and 80 min, the reaction mixture became translucent and then rapidly became opaque, indicating gelation of the supercritical reaction mixture (marked by the first dashed line in Figure 2). As the reaction proceeded the pressure decreased significantly, and after about 170 min (the second dashed line in Figure 2) the reaction pressure remained constant. This suggests that most of the monomer was consumed in the first 90 min after the reaction temperature (60 °C) was reached (i.e., between the dashed lines in Figure 2). Because the molar volume for a vinyl monomer is usually higher than the molar volume for the corresponding polymer (i.e., ΔV_{polym} is negative), one might expect that a pressure drop would always be observed in these reactions, but this is not the case. For example, Canelas and DeSimone studied the dispersion polymerization of MMA in $scCO_2$ at constant monomer concentration, and found that ΔP could be negative, zero, or positive, depending on the initial reaction pressure.[50] Beckman has rationalized this behavior in terms of the nonideality of the solutions, in particular by the fact that the mixing terms, ΔV_m, are nonzero.[51] Figure 3 shows the variation in the pressure change, ΔP (i.e., $P_i - P_f$ at 60 °C), for this series of TRIM polymerizations as a function of the initial reaction pressure at 60 °C (P_i). At lower initial reaction pressures (P_i < 2800 psi), a small net increase in pressure was observed after polymerization. At intermediate pressures ($P_i \sim$ 2700−3000 psi), ΔP was approximately zero. At higher reaction pressures (P_i > 2800 psi), ΔP became increasingly negative. In general, ΔV_m will be a function of pressure, temperature, and the amount of monomer initially present in the system, $[M]_0$.[51] In the present system, T and $[TRIM]_0$ were kept constant, and the relationship between P_i and ΔP was found to be approximately linear (Figure 3).

In evaluating the effect of pressure on these reactions, there are in principle three different pressure variables which could be used. The initial pressure of the system at room temperature (P_0 in Figure 2a) is a poor measure

(50) Canelas, D. A.; DeSimone, J. M. *Macromolecules* **1997**, *30*, 5673−5682.
(51) Lepilleur, C.; Beckman, E. J. *Macromolecules* **1997**, *30*, 745−756.

Table 1. Effect of CO_2 Pressure on Physical Properties of Macroporous Cross-Linked TRIM Monoliths[a]

	P_i (psi)[b]	P_f (psi)[c]	ΔP (psi)[d]	surface area (m^2/g)[e]	micropore surface area (m^2/g)[e]	micropore surface area (%)[e]	absolute density (g/cm^3)[f]	median pore diameter (nm)[g]	intrusion volume (cm^3/g)[g]	N_2 sorption pore volume (cm^3/g)[h]
1	1910	2200	290	279	142	50.9	1.291	45.2	0.832	0.485 (0.342)
2	1930	2330	400	298	123	41.1	1.264	41.0	0.843	0.506 (0.421)
3	2250	2350	100	162	37	23.0	1.279	51.3	0.870	0.404 (0.349)
4	2060	2470	410	176	60	33.8	1.242	73.7	0.885	0.357 (0.289)
5	2030	2510	480	138	37	27.1	1.301	63.4	0.915	0.239 (0.202)
6	2570	2600	30	94	13	14.0	1.276	65.1	0.908	0.325 (0.312)
7	2960	2900	−60	167	33	19.8	1.258	48.0	0.907	0.479 (0.434)
8	3120	2950	−170	146	19	13.0	1.271	48.6	0.901	0.478 (0.449)
9	3870	3130	−740	174	23	13.6	1.302	43.2	0.858	0.503 (0.473)
10	4100	3150	−950	167	26	15.7	1.329	44.6	0.862	0.490 (0.458)
11	4030	3170	−860	161	19	11.6	1.273	46.9	0.865	0.563 (0.538)
12	5060	3520	−1540	219	33	14.9	1.259	44.2	0.844	0.681 (0.633)
13	5070	3550	−1520	269	63	23.3	1.271	42.0	0.785	0.705 (0.619)
14	5380	3650	−1730	253	65	25.7	1.289	40.2	0.773	0.695 (0.636)
15	6020	3900	−2120	304	94	31.1	1.271	36.8	0.760	0.761 (0.671)

[a] Reaction conditions: TRIM (6.06 g), AIBN (2% w/w based on TRIM), 60 °C, 4 h. [b] Initial pressure recorded at 60 °C before reaction (± 40 psi). [c] Pressure recorded at 60 °C after reaction was complete (± 15 psi). [d] $\Delta P = P_f - P_i$. [e] Measured by N_2 adsorption−desorption using the Brunauer−Emmett−Teller method. [f] Measured by helium pycnometry. [g] Measured by mercury intrusion porosimetry over the pore size range 7 nm − 100 μm. [h] Calculated from adsorption branch of isotherm, figure in parentheses calculated from desorption branch of isotherm.

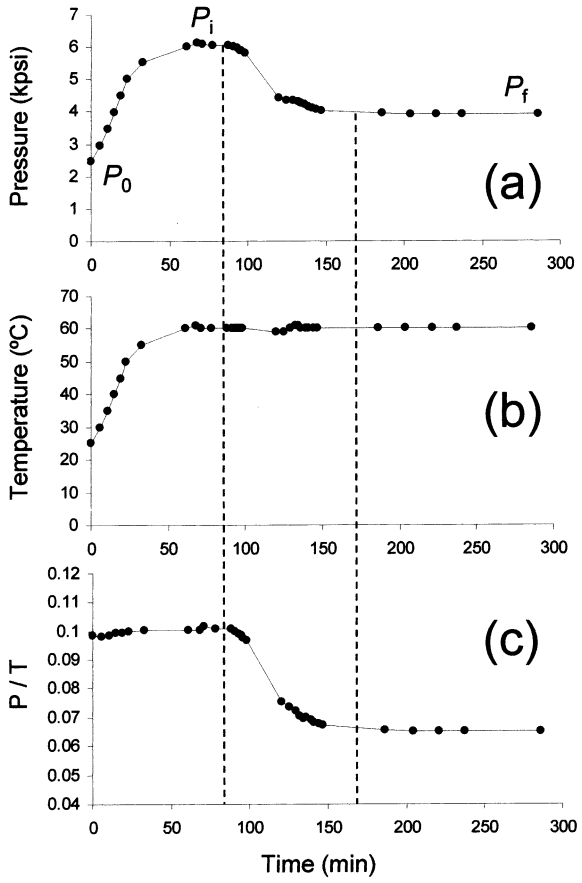

Figure 2. Illustrative plots showing the variation in (a) pressure, (b) temperature, and (c) P/T as a function of reaction time for sample 15.

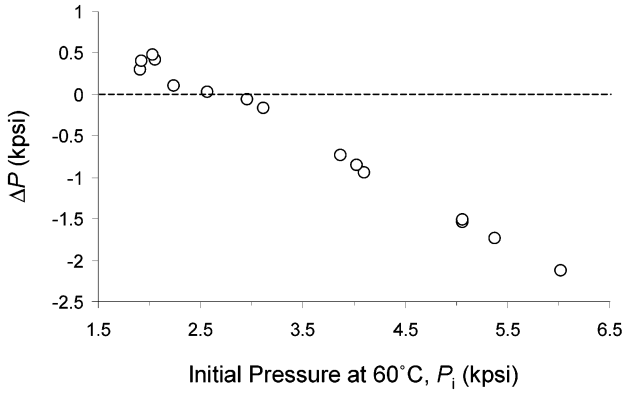

Figure 3. Plot showing the change in pressure, ΔP, ($P_f - P_i$), as a function of the initial reaction pressure, P_i.

of the solvent environment because CO_2 exists in the *liquid* state below 31.1 °C. As such, any reactions where the vessel is partially filled with CO_2 before heating give roughly constant values for P_0 (i.e., the liquid vapor pressure for CO_2), despite the fact that the volume of CO_2 (and the subsequent density in the supercritical state) varies significantly from reaction to reaction. The initial reaction pressure at 60 °C, P_i, is a better choice, but we did not use this variable for the following reasons: (i) P_i might be affected by exotherms caused by the polymerization;[52] (ii) inaccuracies might arise in the determination of P_i because thermal equilibrium was being attained; (iii) some small degree of polymerization may already have occurred as this temperature was reached; and (iv) the solutions are not ideal, and thus ΔV_m varies as a function of P_i. As can be seen in Figure 2a, a constant pressure was measured in the reactor after the polymerization was complete. We therefore considered the final reaction pressure at 60 °C, P_f, to be the best overall measure of the CO_2 solvent environment for the reaction. Considering that the monomer conversion was 95−100% in these reactions, P_f is a better approximation of the pressure arising from the neat supercritical porogen. The value of P_f was also much less subject to errors in measurement because, unlike P_i, it could be determined after the polymerization reaction was complete and the system was at a constant and stable temperature (Figure 2b). Although P_f was chosen as the pressure variable in these studies,

(52) In fact, the temperature of the reactor was measured (by an internal thermocouple) to be fairly constant after the reaction temperature was reached (see for example Figure 2). Nonetheless, this does not preclude the possibility of a brief increase in temperature due to autoacceleration that might influence the value of P_{max} while not being detected by the thermocouple (which measures the average temperature of the whole system).

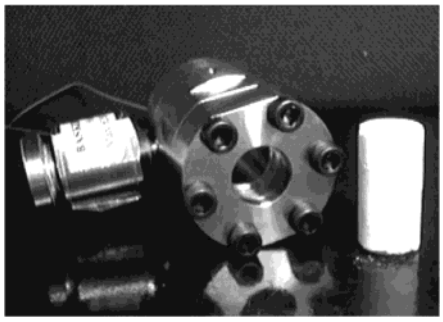

Figure 4. Porous polyTRIM monolith next to the reactor in which it was produced. The material conformed closely to the internal dimensions of the reaction vessel and no noticeable shrinkage was observed.

it should be noted that the qualitative trends observed are in fact the same if one plots the variation in polymer properties as a function of P_i. This is because of the approximately linear relationship between P_i and P_f (Figure 3).[53]

Synthesis of Porous PolyTRIM Monoliths using $scCO_2$: Effect of CO_2 Pressure on Polymer Morphology. Table 1 lists the characterization data for a series of polyTRIM materials synthesized over a range of CO_2 pressures. Because CO_2 is so volatile, the porogen was removed by simple depressurization at the end of the reaction. No additional washing or drying steps were carried out after polymerization, although for applications where small quantities of monomer residue pose a problem (e.g., biomedical materials), one could perform an in situ supercritical fluid extraction step after polymerization.[54−56] All materials were obtained as dry, white, continuous monoliths (Figure 4) that conformed closely to the internal bore of the reaction vessel (i.e., there was little or no apparent shrinkage away from the vessel walls). Each of the materials was characterized by mercury intrusion porosimetry (to measure macropore intrusion volumes and macropore diameters), nitrogen adsorption−desorption analysis (to calculate BET surface areas, micropore surface areas, and pore volumes), and by helium pycnometry (to obtain absolute densities).

(1) Surface Area. Figure 5 shows a plot of total BET surface area (closed circles) and micropore surface area (open circles) for samples 1−15 as a function of the CO_2 pressure (P_f). In the pressure range 2600−4000 psi, there was an approximately linear increase in the total BET surface area as the reaction pressure was increased. This is similar to the trend observed for porous TRIM/MMA copolymer beads synthesized by suspension polymerization using $scCO_2$ as the porogen.[35] Conversely, in the pressure range 2200−2600 psi there was an abrupt linear increase in total BET surface area as the pressure was *decreased* (Figure 5). This gave rise to a distinct minimum in surface area at a pressure of approximately 2600 psi. This effect was *not* observed

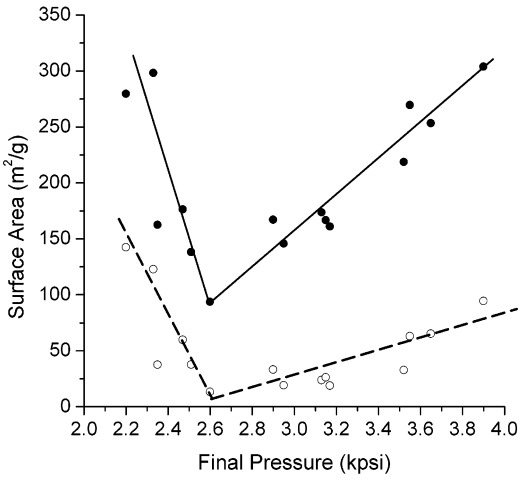

Figure 5. Variation in total BET surface area (●) and micropore surface area (○) as a function of CO_2 pressure, P_f.

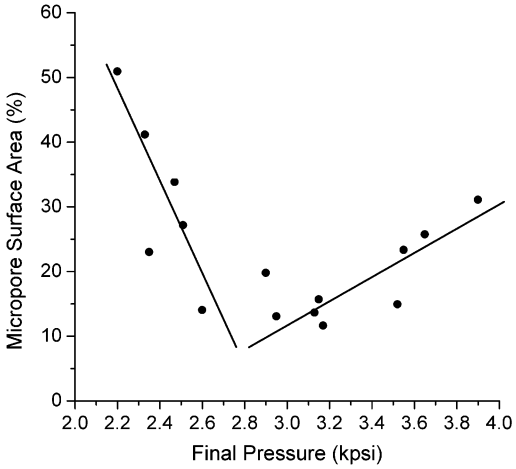

Figure 6. Variation in percentage micropore surface area (i.e., (micropore area/total surface area) × 100) as a function of CO_2 pressure, P_f.

in our suspension polymerization experiments, although those preliminary studies did not explore the low-pressure regime in any detail.[35] Figure 6 shows a plot of the percentage micropore surface area in the samples as a function of CO_2 pressure: this plot also shows a minimum at pressures of around 2600−2700 psi. At the lowest reaction pressure (sample 1, 2200 psi), 50.9% of the total surface area could be accounted for by micropores. At 2600 psi (sample 6), only 13% of the surface area arose from micropores. At the highest reaction pressure studied (sample 15, 3900 psi), the percentage micropore surface area increased again to 31.1%.

Figure 7 shows N_2 adsorption−desorption isotherms for samples 1, 6, and 15. All three samples gave rise to incomplete type II isotherms with type H3 hysteresis loops, similar to the sorption isotherms observed for polyTRIM materials synthesized using butyl acetate as the porogen at relatively low TRIM concentrations (25−33% w/w with respect to the porogen).[18] In comparing these data, it should be noted that the materials produced by Rohr et al.[18] were synthesized by suspension polymerization and that one might expect differences in swelling behavior and polymer shrinkage due to interfacial effects that are absent in the case of monolithic materials.[32,57]

(53) The overall trends and conclusions are also much the same if one plots polymer properties as a function of the CO_2 density (as calculated from P_f).

(54) McHugh, M. A.; Krukonis, V. J. *Supercritical Fluid Extraction*; 2nd ed.; Butterworth-Heinemann: Stoneham, MA, 1994.

(55) Ma, L.; Zhang, L.; Yang, J. C.; Xie, X. M. *J. Appl. Polym. Sci.* **2002**, *86*, 2272−2278.

(56) Kemmere, M.; van Schilt, M.; Cleven, M.; van Herk, A.; Keurentjes, J. *Ind. Eng. Chem. Res.* **2002**, *41*, 2617−2622.

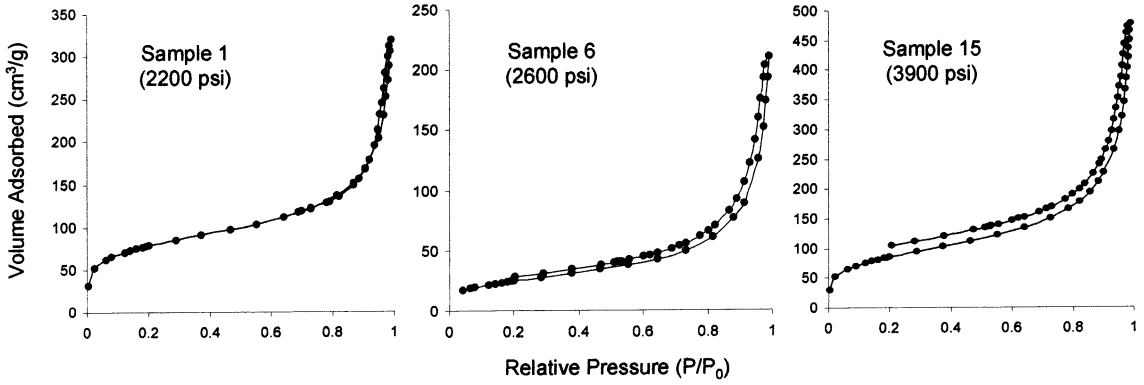

Figure 7. N_2 adsorption−desorption isotherms for (a) sample 1 (SA = 279 m^2/g); (b) sample 6 (SA = 94 m^2/g); and (c) sample 15 (SA = 304 m^2/g).

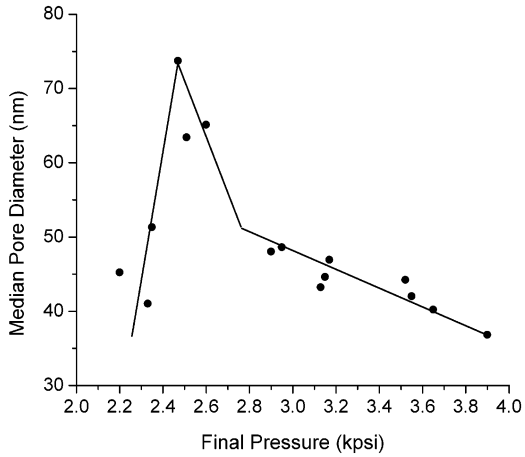

Figure 8. Variation in median pore diameter (nm) as measured by mercury intrusion porosimetry over the range 7 nm − 100 μm as a function of CO_2 pressure, P_f.

(2) Macropore Diameter and Polymer Morphology. Figure 8 shows the variation in macropore diameter for samples 1−15 as a function of pressure, as measured by mercury intrusion porosimetry. It should be noted that intrusion porosimetry measures pores in the size range 7 nm to 100 μm, so any pores smaller than about 7 nm are *not* accounted for by this method. Figure 7 exhibits a maximum in the median mesopore/macropore diameter (~75 nm) at a pressure of around 2600 psi. It should be noted that the pore size distributions in these samples (see below) are broad: as such, the changes in the median pore diameter measured by mercury intrusion porosimetry reflect general shifts in the position of the pore distribution envelope, rather than the position of a well-defined, sharp peak. Careful study of the samples by scanning electron microscopy (SEM) did not reveal any obvious trends in the overall polymer morphology as a function of CO_2 pressure. Clearly, the large variations in the porous properties of these materials result from structural changes on a length scale that is too small to be studied by SEM. In this respect, the structural changes caused by varying the CO_2 solvent density are more subtle than the changes in morphology observed when the monomer concentration is varied, the latter of which can be clearly identified by SEM.[33,34] Figure 9 shows a representative SEM

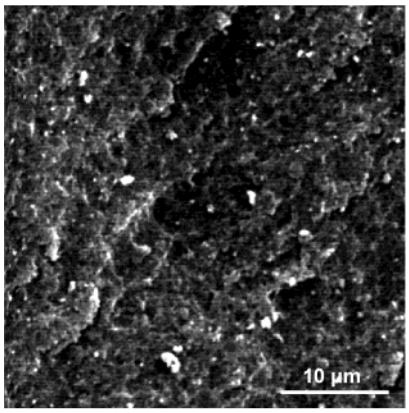

Figure 9. Electron micrograph showing polymer morphology for sample 15 (scale bar = 10 μm).

image, as recorded for sample 15. Analysis of the materials by atomic force microscopy (AFM) revealed structural features on a much smaller length scale. Figure 10 shows a series of three AFM images (1 μm × 1 μm) recorded for samples 1, 6, and 15. The images suggest that sample 6 contained a greater degree of "coarse" pore structure in the 50−200 nm range. This is consistent with the fact that sample 6 exhibited the lowest surface area and the largest median macropore diameter (see also Figure 8). The differences in morphology observed by AFM in our samples were not nearly as marked as the changes in surface morphology reported by Neves et al. for poly(styrene-divinylbenzene) copolymers produced by suspension polymerization.[58] In that study, mixtures of toluene and heptane (either 70:30 or 30:70 v/v) were used as the porogen and it was found that much coarser polymer morphology was observed when the heptane ratio was high.[58] Again, this probably reflects the fact that the pressure-dependent solvent quality of the SCF porogen in our experiments varies in a comparatively subtle way.

(3) Pore Volume. A shallow maximum was also observed at a reaction pressure of around 2600 psi for the total intrusion volume (i.e., the macropore and mesopore volume for pores larger than 7 nm), as measured by mercury intrusion porosimetry (squares in Figure 11). The trend in pore volume as calculated by N_2 sorption followed the reverse trend and a pro-

(57) Otake, K.; Webber, S. E.; Munk, P.; Johnston, K. P. *Langmuir* **1997**, *13*, 3047−3051.

(58) Neves, M.; Coutinho, F. M. B.; Dias, M. L.; Simao, R. A.; Achete, C. A. *J. Appl. Polym. Sci.* **2002**, *84*, 541−551.

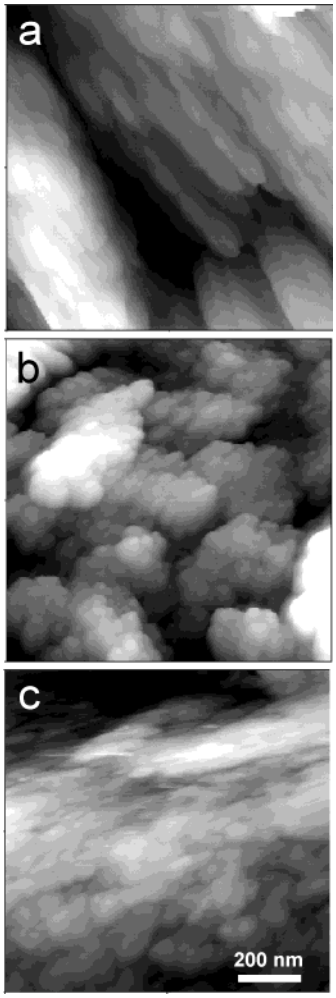

Figure 10. AFM images for (a) sample 1; (b) sample 6; and (c) sample 15. Image size = 1 μm × 1 μm in each case.

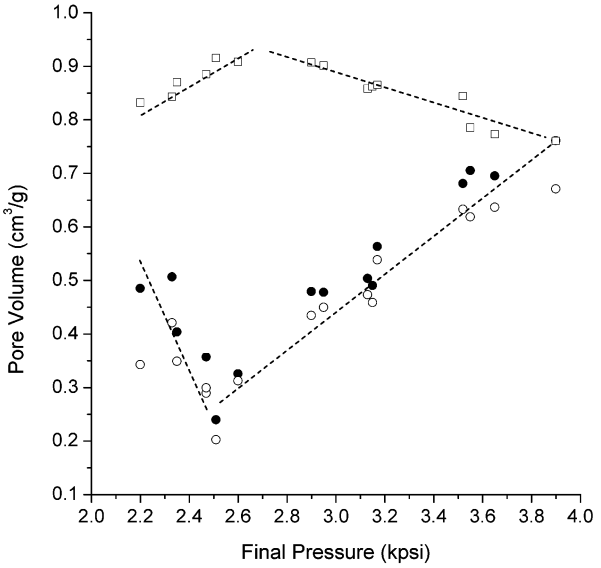

Figure 11. Variation in total intrusion volume (mercury intrusion porosimetry, □, open squares) and N_2 sorption pore volume (circles) as a function of CO_2 pressure, P_f. Closed circles (●) calculated from adsorption loop, open circles (○)calculated from desorption loop of isotherm.

nounced minimum was observed at a similar pressure (circles in Figure 11). From consideration of the mass of monomer added to the reactor (6.06 g), the absolute

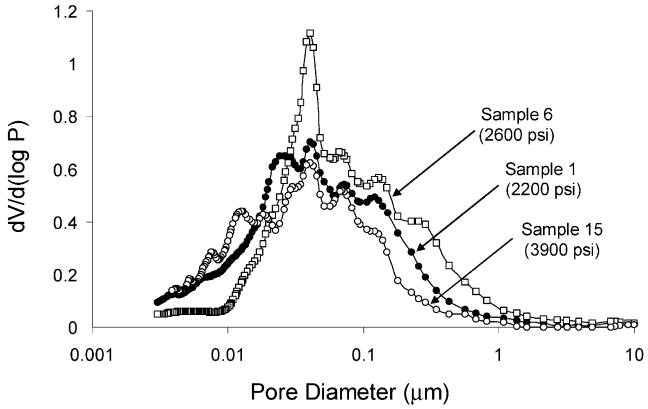

Figure 12. Pore size distributions, as measured by mercury intrusion porosimetry, for samples 1, 6, and 15.

density of the polyTRIM material (1.28 g/cm^3, see below) and the reactor volume (10 cm^3), one can calculate the total volume of the resultant polymer phase to be approximately 6.06/1.28 = 4.73 cm^3. Thus, one can estimate the total pore volume, V_{tot}, expected for these materials to be approximately (10 − 4.73)/6.06 = 0.87 cm^3/g.[59] Neither gas sorption nor mercury intrusion porosimetry alone gives a full picture of the porosity in materials of this type. Intrusion porosimetry does not detect pores smaller than 7 nm, while the pore volumes measured by N_2 sorption−desorption can be ascribed mostly to pores smaller than about 200 nm. As a consequence, neither of these measurements can fully account for the porosity in the samples, particularly when the pore size distribution is broad. In this series, sample 6 comes closest to being a purely mesoporous−macroporous material (micropore surface area ∼13%), and in this case the measured intrusion volume (0.908 cm^3/g) is quite close to the "theoretical" value of 0.87 cm^3/g. Similarly, gas sorption gives a more realistic measure of the total pore volume in those materials which have a higher proportion of micropores (i.e., the samples produced at higher pressures, samples 12−15). Overall, intrusion porosimetry gives a better measure than gas sorption of the total pore volume in these predominantly mesoporous−macroporous materials.

(4) Macropore/Mesopore Size Distributions. Figure 12 shows mercury intrusion pore size distributions for samples 1, 6, and 15 (synthesized at 2200, 2600, and 3900 psi, respectively). It is clear from these plots that samples 1 and 15 (synthesized at the lowest and the highest CO_2 pressures, respectively) contained a higher proportion of mesopores (diameters <50 nm) than did sample 6 which was synthesized at 2600 psi. It is also clear that the sample synthesized at the highest CO_2 pressure (sample 15) contained a somewhat greater proportion of mesopores (and a lower proportion of large macropores with diameters >500 nm) than did the sample produced at the lowest pressure (sample 1). These pore size distributions suggest that the polymers may be useful in a number of applications, particularly those where it is desirable to have large, "flow-through" macropores (>100 nm) interconnected with smaller pores in the mesopore and micropore size range.[22,23,32] Moreover, these data show how it is possible to shift

(59) This assumes a monomer conversion of 100%; the actual monomer conversion was slightly lower (95−100%).

this distribution of pore sizes over a significant range by varying the CO_2 pressure, thus allowing the relative proportions of micro-, meso-, and macropores in the materials to be tuned for a given application.

(5) Absolute Density. The absolute density (or "skeletal" density) as measured by helium pycnometry did not vary significantly as a function of CO_2 pressure. The average absolute density for the cross-linked polyTRIM material was found to be 1.28 ± 0.02 g/cm^3. The absolute density of the polymer was significantly higher than the density of the monomer, TRIM (1.06 g/cm^3), as expected for a system where ΔV_{polym} is negative. The fact that the absolute density did not vary much from sample to sample suggests the absence of any significant closed porosity (i.e., that all of the pores were interconnected).

Rationalization of Pressure Effect. All of the data presented in Figures 5−12 are consistent with the existence of a minimum in microporosity (small pores) and a maximum in macroporosity (large pores) for samples prepared at CO_2 pressures close to 2600 psi. As the reaction pressure was increased from 2600 to 4000 psi, the macropore volume fell somewhat (Figure 11) while the micropore/mesopore volume increased considerably. When the reaction pressure was decreased from 2600 to 2200 psi, the reverse trend was observed. The resultant effect on the polymer surface area is summarized in Figures 5 and 6.

The existence of maxima and minima in the porous properties of these materials is not readily accounted for by a simple correlation with CO_2 pressure (or density). Thus, we rationalize the variation in polymer morphology by considering the phase behavior in two different pressure regimes.

Pressure Range 2600−4000 psi. Over this pressure range there was a large (∼300%) increase in total surface area, an increase in micropore surface area, an increase in the N_2 sorption pore volume, a decrease in the average macropore diameter, and a (relatively small) decrease in the total intrusion volume (i.e., the volume occupied by mesopores and macropores with diameters greater than 7 nm). We attribute this trend to increased solvation as the CO_2 density is raised, which causes polymer phase separation to occur at a somewhat later stage in the reaction. This gives rise to the formation of a finer pore structure with less in-filling between individual agglomerated microgel particles, as argued by Sherrington for the case of conventional organic solvent porogens.[10,18] This effect on the morphology occurs at a size range that is too small to be observed by SEM, but that is at least suggested by AFM imaging (Figures 9 and 10). The decrease in the average pore diameter leads to an increase in the number of micropores and an increase in the BET surface area. The decrease in intrusion volume as measured by mercury porosimetry arises from the fact that this technique cannot detect pores smaller than about 7 nm, and that an increasing percentage of the pore volume falls below this limit (see Figure 12, which gives a hint of this for samples 1 and 15 at the low pore-diameter cutoff). The same explanation can be used to rationalize the variation in surface area observed for macroporous TRIM/MMA copolymer beads synthesized by suspension polymerization using $scCO_2$ as the porogen.[35] We attribute this behavior primarily to the variation in the CO_2 solvent properties as a function of pressure (i.e., density). The *volume* of compressed CO_2 at the end of each polymerization can be assumed to be approximately constant for each experiment because the reactor volume is fixed. This is true even though the *molar* ratio of monomer to CO_2 changes significantly from experiment to experiment. This significant variation in density and molar ratio (or molality) at a constant volume is a unique feature of experiments involving highly compressible fluids. We believe that the effects of CO_2 density on the pore structure over this pressure range can be explained by the fact that the system is very sensitive to the porogen solvent quality, which influences the mechanism of phase separation, nucleation, aggregation, and pore formation.[10] Similar effects have been documented for conventional organic solvent porogens. For example, Peters et al. observed a dramatic porogen effect on the structure of copolymer monoliths synthesized from EDMA, butyl methacrylate, and 2-acrylamido-2-methyl-1-propanesulfonic acid (AMPS).[26] A ternary porogen mixture was used consisting of 10 wt % water and 90 wt % of a mixture of 1-propanol and 1,4-butanediol. The average pore size of the monoliths was tuned by controlling the ratio of the two alcohols. Somewhat surprisingly, the porous structure was found to be *extremely* sensitive to the porogenic solvent composition: for example, when the proportion of propanol was increased from 55 wt % to 63 wt %, the average pore size decreased from ∼5000 nm to just 150 nm.[26] The results suggested that this could be attributed to the degree of solvation for the AMPS moieties, since the effect was more pronounced at higher AMPS incorporations. In a similar way, the average pore size in EDMA/glycidyl methacrylate copolymer monoliths was controlled by using a cyclohexanol/dodecanol porogen mixture and varying the ratio of the two alcohols.[60] Xie et al. studied a homologous series of alcohols (methanol − dodecanol) mixed with dimethyl sulfoxide as porogens for the preparation of poly(acrylamide-*co*-methylenebisacrylamide) monoliths and found that the average pore size increased significantly with increasing chain length of the porogenic alcohol.[61] Each of these studies illustrates the fact that the structure of highly cross-linked, permanently porous cross-linked polyacrylates and polymethacrylates can be very sensitive to the precise nature of the porogenic diluent. As such, the use of $scCO_2$ offers a potential advantage for controlling structure in these materials because the solvent properties can be fine-tuned with pressure (i.e., a fairly large change in pressure leads to a relatively subtle change in the solvent strength).[39]

Pressure Range 2200−2600 psi. The arguments presented above are, of course, contradicted by the sharp increase in total BET surface area and micropore volume that is observed when the CO_2 pressure is reduced over the range 2600−2200 psi. We rationalize this by noting that the system is approaching the demixing pressure (i.e., at pressures below about 2000 psi at 60 °C, TRIM and CO_2 are no longer fully miscible at this concentration). Thus, at pressures approaching

(60) Svec, F.; Fréchet, J. M. J. *Macromol. Symp.* **1996**, *110*, 203.
(61) Xie, S. F.; Svec, F.; Fréchet, J. M. J. *J. Polym. Sci. Polym. Chem.* **1997**, *35*, 1013−1021.

2000 psi, one might expect pronounced solute−solute clustering or "local composition enhancement", as these are known to be common in supercritical solvents at reduced solvent densities.[62,63] Under those conditions, monomer−monomer clustering could increase the effective monomer concentration during microgelation. One might also predict that very low solvent quality would also strongly influence the partitioning of the monomer from the porogen phase into the swollen polymer phase.[64−66] We suggest that these factors override any effects relating to phase separation later in the reaction, and that poor solvent quality could lead to local molecular environments that are equivalent to a higher monomer concentration (even though the volume of monomer added to the reactor is constant in all experiments). In essence, the effective monomer concentration may differ from the actual monomer concentration at pressures close to the demixing pressure. A number of previous studies have invoked clustering[62,67−69] or substrate partitioning[70,71] to explain changes in reaction rates or in product selectivity observed for organic reactions conducted in $scCO_2$ at differing solvent densities. A similar rationalization in our experiments is consistent with the fact that the average pore size and surface area for materials produced by this route are extremely sensitive to the monomer concentration.[33,34]

It is intriguing to note that the various maxima and minima in the porous properties of this series of materials occur at pressures (2600−2700 psi) which are close to the pressure at which a minimum in ΔP is observed (Figure 4). Indeed, the sample which had the lowest total surface area and the lowest percentage of micropores (sample 6) was prepared under conditions where ΔP was just +30 psi. Moreover, all of the samples synthesized in the low-pressure regime (where surface area decreased with increasing pressure) were formed under conditions where ΔP was positive. In the high-pressure regime (where the surface area increased with increasing pressure), ΔP was always negative. The physical significance of this (if any) is not clear at this stage, but it is very likely that the magnitude and sign of ΔV_m would also affect the evolution of the pore structure in these materials, particularly in the earlier stages of the polymerization.

Conclusions

We have shown that it is possible to fine-tune the porous properties for cross-linked polyTRIM materials synthesized using $scCO_2$ as the porogen by varying the fluid density. Surface area and average pore size exhibit distinct minima and maxima, respectively, at a certain reaction pressure (around 2600 psi in this particular system). Although the precise mechanism of pore formation in these materials is extremely complicated, the results suggest that two separate pressure regimes can be considered: (i) lower pressures close to the monomer−solvent demixing pressure where clustering and monomer partitioning may occur; and (ii) higher pressures where the monomer is completely miscible with the SCF and clustering effects are less pronounced. These results illustrate how it is possible to tailor materials' properties by varying the SCF solvent density in a manner which is not possible using conventional liquid organic solvents. Future studies will focus on the applications of materials prepared by this route, particularly in the area of chromatography.

Acknowledgment. We thank EPSRC for funding (GR/23653 and GR/R15597). A.I.C. acknowledges the support of the Royal Society through the provision of a Research Fellowship. We thank Dr. Mathias Brust for advice and helpful discussions.

CM020979I

(62) Brennecke, J. F.; Chateauneuf, J. E. *Chem. Rev.* **1999**, *99*, 433−452.
(63) Kim, S. W.; Johnston, K. P. *AIChE J.* **1987**, *33*, 1603−1611.
(64) Brantley, N. H.; Bush, D.; Kazarian, S. G.; Eckert, C. A. *J. Phys. Chem. B* **1999**, *103*, 10007−10016.
(65) Kazarian, S. G.; Vincent, M. F.; West, B. L.; Eckert, C. A. *J. Supercritical Fluids* **1998**, *13*, 107−112.
(66) Condo, P. D.; Sumpter, S. R.; Lee, M. L.; Johnston, K. P. *Ind. Eng. Chem. Res.* **1996**, *35*, 1115−1123.
(67) Oakes, R. S.; Clifford, A. A.; Rayner, C. M. *J. Chem. Soc., Perkin Trans. 1* **1999**, 917−941.
(68) Roberts, C. B.; Chateauneuf, J. E.; Brennecke, J. F. *AIChE J.* **1995**, *41*, 1306−1318.
(69) Roberts, C. B.; Zhang, J.; Chateauneuf, J. E.; Brennecke, J. F. *J. Am. Chem. Soc.* **1995**, *117*, 6553−6560.
(70) Weinstein, R. D.; Renslo, A. R.; Danheiser, R. L.; Tester, J. L. *J. Phys. Chem. B* **1999**, *103*, 2878−2887.
(71) Rose, P. M.; Clifford, A. A.; Rayner, C. M. *Chem. Commun.* **2002**, *2002*, 968−969.